

Received 19 July 2024, accepted 15 August 2024, date of publication 21 August 2024, date of current version 4 September 2024.

Digital Object Identifier 10.1109/ACCESS.2024.3447275

## RESEARCH ARTICLE

# Upper Limb Movement Prediction Based on Segmented sEMG Signals

HAO YAN<sup>1,2</sup>, XINGAO LI<sup>1</sup>, ZHONGLIANG SHI<sup>1</sup>, AND SHUYUAN WANG<sup>2</sup>

<sup>1</sup>Key Laboratory of Intelligent Industrial Equipment Technology of Hebei Province, Hebei University of Engineering, Handan 056038, China

<sup>2</sup>Collaborative Innovation Center for Modern Equipment Manufacturing of Jinan New Area, Hebei University of Engineering, Handan 056038, China

Corresponding author: Hao Yan (yanhao@hebeu.edu.cn)

This work was supported in part by the Hebei Natural Science Foundation under Grant E2022402059, in part by the Science and Technology Research Project of Hebei Province Higher Education Institutions under Grant QN2023122, in part by the Key Technologies Research and Development Programme under Grant SQ2019YFB130349, and in part by the University-Industry Collaborative Education Programme of the Ministry of Education under Grant 22097118175453.


This work involved human subjects or animals in its research. Approval of all ethical and experimental procedures and protocols was granted by the Medical College of Hebei University of Engineering, and performed in line with the Declaration of Helsinki the World Medical Association.

**ABSTRACT** Motion intent recognition research is one of the key challenges in achieving human-robot collaboration in rehabilitation robots. In the traditional method, intention recognition is performed based on the complete sEMG, however, due to the muscle atrophy of stroke patients, the complete sequences are not captured at the early stage of rehabilitation, so in this paper, three sEMG segments of 1/2, 1/4, and 1/8 of three selected activity of daily living (ADL) movements of the upper limb are investigated, respectively, and comparing with the complete sEMG sequences, a novel method of motor intention prediction is proposed. In order to achieve optimal recognition accuracy and speed, the Kernel Extreme Learning Machine (KELM) algorithm optimized by the Sparrow Search Algorithm (SSA) algorithm was used for prediction. It was found that the SSA-KELM algorithm based on segmented sEMG has better recognition accuracy and recognition speed in each segment compared to other algorithms. The recognition accuracy in 1/8 sEMG segments is 98.4%, and the recognition time is 0.0102s, which shows how well the method works and what it means for rehabilitation robots working together with people.

**INDEX TERMS** Segmental sEMG, motion intent prediction, SSA-KELM, human-robot collaboration.

## I. INTRODUCTION

Stroke is one of the leading causes of long-term disability in the world's population. According to statistics, about 70% to 80% of stroke patients have varying degrees of upper limb motor dysfunction, which greatly affects their independence in daily life [1], [2], [3]. Rehabilitation robots can assist stroke patients with motor training to restore normal limb function [4]. With the continuous development of artificial intelligence, the application of pattern recognition technology in the field of medical rehabilitation is becoming more and more widespread, and it has a positive significance

The associate editor coordinating the review of this manuscript and approving it for publication was Angelo Trotta .

for the closed-loop control of patients' postoperative active rehabilitation [5], [6].

Methods for recognizing motion intention rely on biomechanical and bioelectric signals [7]. The generation of bioelectric signals occurs before a limb moves. We can find the relationship between the signals and movement by collecting and decoding bioelectric signals, which is a very useful way to predict trends in human limb movement.

The sEMG is a physiological electrical signal generated by neuromuscular movement, and the acquisition technology is mature and noninvasive [8], [9]. It can be obtained by electrodes pasted on the skin surface of human muscle parts and correlates with the corresponding muscle activity and movement status with similarity, difference, and repeatability

**TABLE 1.** Summary of the recent work of identifying the motion intention through sEMG.

Reference	Model	sEMG	Motion	Recognition Accuracy	Predicted Effects
[16]	MSISSA-LSSVM	Complete sEMG; 4CH	8* Single Joint	97.098%	No
[17]	ELM	Complete sEMG; 4CH	6* Gesture	94.7% ~ 97.42%	No
[18]	RBF+SOM	Complete sEMG; 8CH	8* Gesture	96.88% ± 2.73%	No
[19]	CNN	Complete sEMG;12CH	2*ADL+2* Single Joint	69.96% ~ 97.57%	No
[20]	BP	Complete sEMG;2CH	6* Gesture	95.46%	No
[21]	TL+CNN+LSTM	Complete sEMG;128CH	30* Gesture	93.73% ± 7.03%	No
This Text	SSA-KELM	Segment sEMG;2CH	3*ADL	Complete sEMG segment: 96.67% 1/2 sEMG segment: 95.75% 1/4 sEMG segment: 96.89% 1/8 sEMG segment: 98.4%	Yes

In TABLE 1, CNN denotes convolutional neural network, SOM denotes Self-organising mapping neural networks.

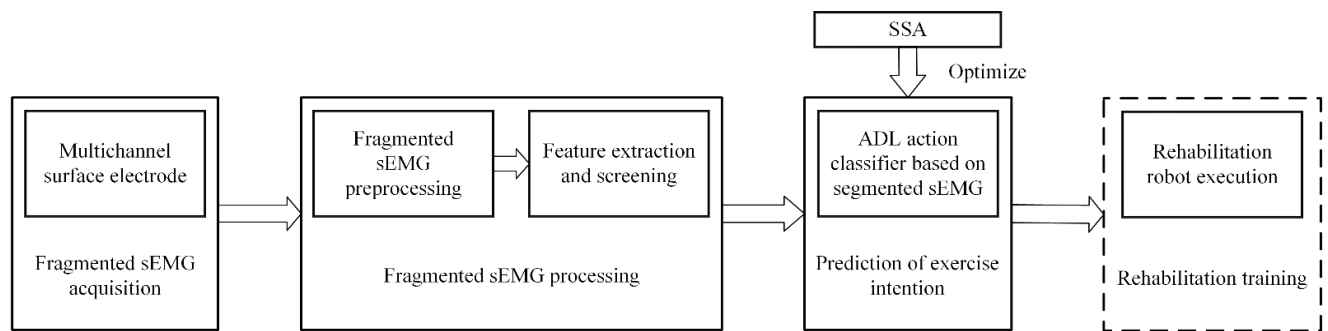


**FIGURE 1.** Segmental sEMG-based upper limb movement intention recognition.

[10], [11], [12]. Therefore, we can classify and recognize movement patterns using the sEMG of muscle groups during human upper limb movement [13], [14], [15].

Motion intent recognition using sEMG signals typically involves two key steps: feature extraction and pattern classification. Chen et al. [16] extracted three features, Root Mean Square (RMS), Integrated Electromyography (iEMG), and Median Power Frequency (MPF), from surface EMG signals, used least squares support vector machines for pattern classification of eight upper limb monoarticular motions, and designed a multi-strategy-based sparrow search algorithm for optimisation of the classifier parameters. They improved the recognition accuracy by 2.835% compared to the original classifier. Shi et al. [17] proposed a combined scheme of cumulative residual entropy and an extreme learning machine (ELM) to classify different hand and wrist movements, and the experimental results verified the real-time performance of the proposed method. Wang et al. [22] used combined kernel principal component analysis to reduce the dimensionality of features. Support Vector Machine (SVM) was used to classify the upper limb movements, and the parameters were optimised using the cuckoo search algorithm, which resulted in a classification accuracy of 95.4% with the feature combination mean absolute value (MAV) + autoregressive coefficient + wavelet packet energy. These works effectively identify the designed motion patterns with different input features and classification models, which are of high research and practical significance. A summary of recent

work on recognizing motor intent by sEMG is shown in TABLE 1.

Currently, action recognition can be divided into two main categories: the first is model-based methods, and the second is data-based machine learning methods [23]. When previous scholars used machine learning methods for action recognition, most of them captured the complete sEMG action sequences and then recognized the actions based on the muscle activation or synergy matrices after the actions occurred [24], [25]. However, they were unable to achieve the effect of action prediction. Simultaneously, when patients use rehabilitation robots for motor training, the limited range of limb movement due to nerve damage frequently hinders the capture of complete sEMG sequences, reducing the robot's capacity to carry out active rehabilitation. This, in turn, impacts the efficacy of rehabilitation. In this paper, we propose a method for motor intention recognition using segmented sEMG, using the KLEM classifier, and using the SSA algorithm for its hyperparameter optimisation, as well as a multi-strategy analysis of muscle group selection, feature filtering, meta-heuristic optimisation algorithm optimisation, and pattern classifier selection, to form a fragmented sEMG-based motor intention recognition system for the upper limb. This method can effectively solve the problem of predicting the patient's behavioural intention and reduce the time delay of the rehabilitation robot, laying the foundation for further active-passive training control. The main content of this paper is shown in FIGURE 1.

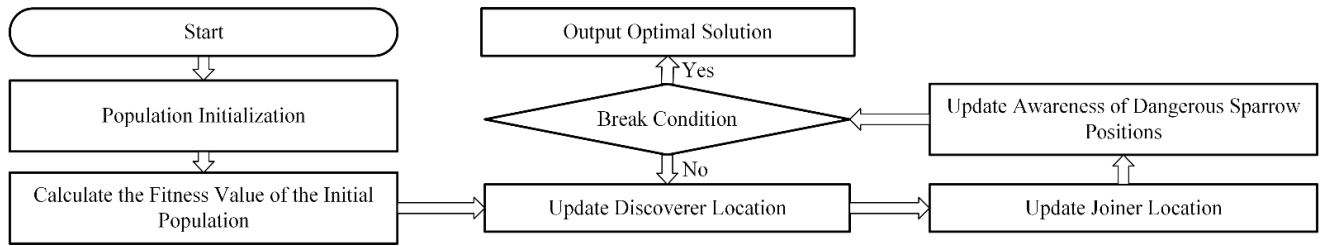


FIGURE 2. SSA Flowchart.

## II. METHOD

### A. SSA ALGORITHM

The SSA was proposed in 2020 as a new population optimisation algorithm derived with reference to sparrow foraging and anti-predation processes [26], [27], which has the advantage of better global exploration and local exploitation to make the sparrows in the population move towards the global optimum and converge quickly near the optimum. The flowchart of SSA is shown in FIGURE 2.

In the modelling process, the position of each sparrow is first established using a matrix with the expression:

$$\begin{pmatrix} X_{1,1} & \cdots & X_{1,d} \\ \vdots & \ddots & \vdots \\ X_{n,1} & \cdots & X_{n,d} \end{pmatrix} \quad (1)$$

where  $n$  is the number of sparrows and  $d$  is the dimension of the variable to be optimised, the fitness can be expressed as:

$$F(x) = \begin{bmatrix} f(x_{1,1}, \cdots, x_{1,d}) \\ \vdots \\ f(x_{n,1}, \cdots, x_{n,d}) \end{bmatrix} \quad (2)$$

where Each row of  $f(x)$  indicates the individual sparrow's fitness. The higher the fitness, the less difficult it is to get food. The optimal individual in the group will be preferred to obtain food during the search process. As a discoverer, it can obtain a larger foraging search range than a joiner and is responsible for guiding the population to find food. During each iteration, the position of the discoverer is updated as follows:

$$x_{i,j}^{t+1} = \begin{cases} x_{i,j}^t \cdot \exp\left(\frac{-i}{\alpha \cdot iter_{MAX}}\right), & R_2 < ST \\ x_{i,j}^t + Q \cdot L, & R_2 \geq ST \end{cases} \quad (3)$$

where  $R_2$  denotes the alert value of the sparrow and  $ST$  denotes the safety threshold.  $x_{i,j}^{t+1}$  denotes the position of the  $i$ th sparrow in the  $j$ th dimension,  $\alpha$  is a [0, 1] random number,  $L$  is a  $1 \times d$  matrix, where each element is 1. Under normal circumstances, when the sparrow's alert value is less than the safety threshold, that is to say, the environment is safe, and it carries out normal hunting. When the sparrow's alert value exceeds the safety threshold, it means there is a danger in the action, and the sparrow will send out an alert to remind the whole group to transmit the information so that the individual can respond.

The positions of the joiners have been updated, as shown below:

$$X_{i,j}^{t+1} = \begin{cases} Q \cdot \exp\left(\frac{X_{worst}^t - X_{i,j}^t}{i^2}\right), & i > n/2 \\ X_p^{t+1} + |X_{i,j}^t - X_p^{t+1}| \cdot A^+ \cdot L, & i \leq n/2 \end{cases} \quad (4)$$

where  $n$  is the number of joiners,  $X_{worst}^t$  is the worst position in the game,  $X_p^{t+1}$  is the globally optimal position.  $i > n/2$  suggests that one of the less adapted  $i$  joiners did not acquire food and its need to search for food elsewhere. In addition, this paper's finder's share is 0.4 for finders, with joiners dynamically adjusting to vigilantes.

When in danger, the pattern of change in the sparrow's position is as follows:

$$X_{i,j}^{t+1} = \begin{cases} X_{best}^t + \beta \cdot |X_{i,j}^t - X_{best}^t|, & f_i > f_g \\ X_{i,j}^t + k \cdot \left(\frac{|X_{i,j}^t - X_{worst}^t|}{(f_i - f_w) + \varepsilon}\right), & f_i = f_g \end{cases} \quad (5)$$

where  $f_g$  is the global optimal fitness value,  $f_i$  is the global worst fitness value,  $X_{best}^t$  is the global optimal position, and  $X_{worst}^t$  is the global worst position.  $k$  and  $\beta$  are random numbers between 0 and 1. Individual fitness values greater than the global optimal fitness value indicate that the sparrow is still far away from the central position, easy to become the target of predators, and more dangerous, while individual fitness values less than the global optimal fitness value indicate that in the vicinity of the central position, the sparrow is aware of the danger and has begun to approach the other sparrows.

### B. KELM MODEL

ELM is a single implicit layer feedforward neural network whose learning objective function  $F(x)$  can be represented by a matrix as follows:

$$F(x) = h(x) \times \beta = H \times \beta = L \quad (6)$$

where  $x$  is the input vector,  $h(x)$  and  $H$  are the hidden layer node outputs,  $\beta$  is the output weight and  $L$  is the desired output. Turning the network training into a linear system solving problem,  $\beta$  is determined according to  $\beta = H^* \times L$ , where  $H^*$  is the generalised inverse matrix of  $H$ . To enhance the stability of the neural network, the regularisation coefficient  $c$

and the unit matrix  $I$  are introduced, and the least squares solution for the output weights is given by

$$\beta = H^T (HH^T + \frac{I}{c})^{-1}L \quad (7)$$

KELM is an improved algorithm based on ELM combined with the kernel function, which improves the predictive performance of the model while retaining the advantages of ELM. Introducing the kernel function into ELM, the kernel matrix is:

$$\Omega_{ELM} = HH^T = h(x_i)h(x_j) = K(x_i, x_j) \quad (8)$$

where:  $x_i, x_j$  is the experimental input vector, then Eq. (9) can be expressed as:

$$F(x) = [K(x, x_1); \dots K(x, x_n)] (\frac{I}{C} + \Omega_{ELM})^{-1}L \quad (9)$$

where:  $(x_1, x_2 \dots x_n)$  is the given training samples,  $n$  is the number of samples,  $K$  is the kernel function, the kernel function selected in this paper is the Gaussian kernel function.

### C. SSA-KELM MODEL

The sparrow optimisation algorithm optimises two parameters of the kernel-limit learning machine: the regularisation coefficient  $c$  and the kernel function parameter  $s$ , resulting in the SSA-KELM model for classification prediction of segmented sEMG signals. The optimisation steps are as follows:

Step 1: Initialise the population. Set the number of sparrows to 20, and randomly generate the initial regularization coefficient  $c$  and kernel function parameter  $s$  to generate the population's initial position.

Step 2: Calculate the range of values for the optimization parameters. Experience leads us to determine the regularisation coefficient  $c$  to be  $(0, 1)$  and the kernel function parameter  $s$  to be  $(-10, 10^5)$ .

Step 3: Establish the SSA-KELM model, calculate the individual sparrow fitness ( $i = 1, 2, \dots, n$ ), and sort the fitness values to identify the current best and worst individuals. The fitness function is:

$$f(x_i) = \sqrt{\frac{1}{n} \sum_{i=1}^n (\hat{d}_i - d_i)^2} \quad (10)$$

where:  $d_i$  is the true value and  $\hat{d}_i$  is the predicted value of the function.

Step 4: Update the sparrow's position according to Eqs. 3-5.

Step 5: Obtain the new sparrow position and individual fitness value; compare the optimal fitness value of the current round with the previous optimal fitness value; and, if the current round is optimal, update the global optimal fitness value with the relevant bits.

Step 6: Stop the loop. When the number of iterations is greater than 30, the optimality search process ends.

Step 7: The optimal training parameters for KELM are obtained, the model is built, and the optimisation process is shown in FIGURE 3.

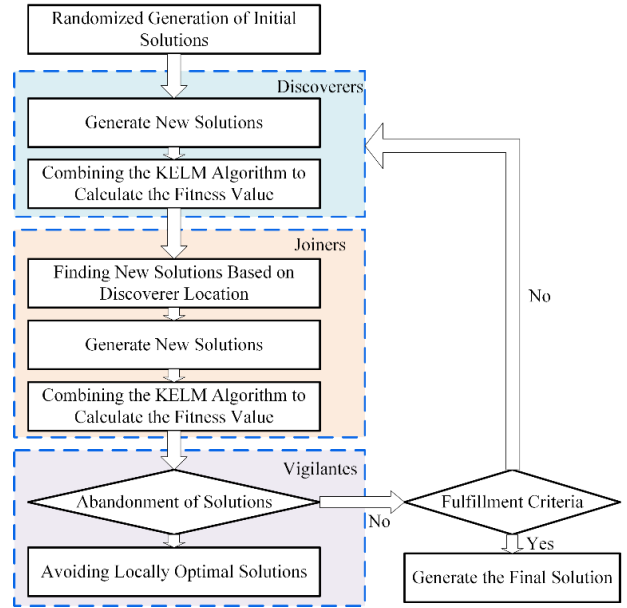


FIGURE 3. Flowchart of SSA optimisation of KELM.

## III. SEMG COLLECTION AND PROCESSING

### A. COLLECTION EQUIPMENT AND ENVIRONMENT

This paper utilized Biosignals, a physiological multidirectional recorder from PLUX, Portugal, to acquire raw sEMG data. The hardware includes 8-channel (CH) wireless acquisition sensors for physiological signals, and the software includes data acquisition, visualization processing, and real-time display modules, as shown in FIGURE 4.

In this paper, we collected sEMG from six healthy participants, four males and two females, with the right limb serving as the habitual upper limb. The collection protocol was strictly based on the Declaration of Helsinki, and all subjects read and signed an informed consent form agreeing to the use of their personal data for the study.

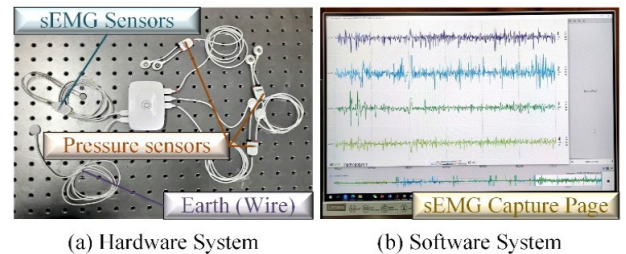
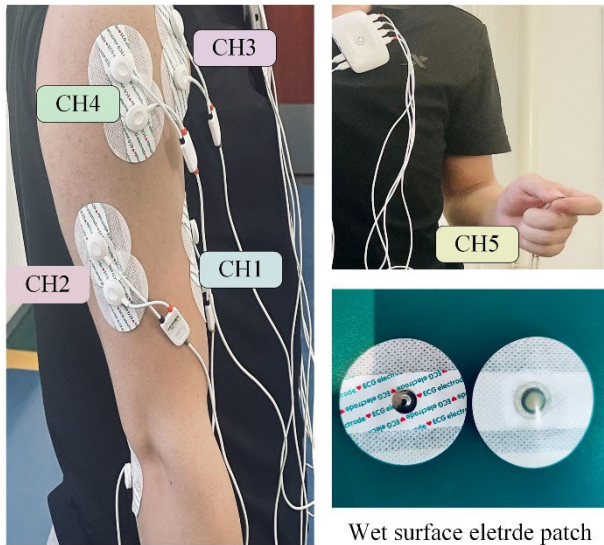


FIGURE 4. Biosignals signal acquisition system.

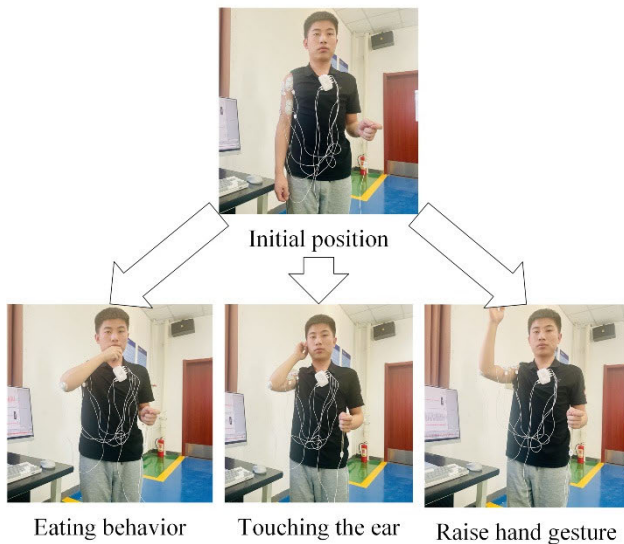
Each subject underwent adequate muscle relaxation prior to acquisition. Before attaching the electrodes, the corresponding muscle area was wiped with 75% alcohol in order to remove surface oils and improve conductivity, thereby reducing noise and improving the signal-to-noise ratio. Wet electrodes containing electrolyte gel were used for

TABLE 2. Collection channel configuration.

Channel Settings	Equivalent Fleet	Subject of Collection	Sampling Rate
CH1	The biceps brachii	Healthy human right upper limb	2048Hz
CH2	The triceps brachii		
CH3	Anterior deltoid muscle		
CH4	Middle deltoid muscle	Healthy human left finger	
CH5	-		



(a)



(b)

FIGURE 5. Electrode attachment position and movement schematic.

acquisition, and electrode patches were attached to the centre of each muscle along its fibre direction.

All tests were conducted in the same environment with Windows 10, a 64-bit operating system, an Intel Core

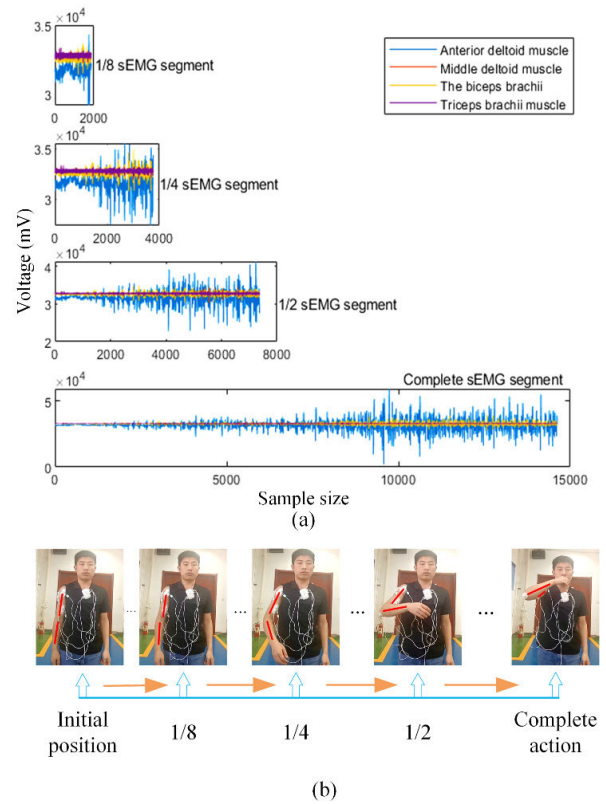


FIGURE 6. Schematic illustration of eating action segments.

i7-9750H @ 2.60GHz six-core processor, and MATLAB R2018b as the integrated development platform.

B. SEMG ACQUISITION AND MUSCLE SELECTION

Based on the principles of “convenient collection, large muscle area, long distance, and avoiding overlap” [28]. Three muscle groups, namely, deltoid, the biceps, and triceps, were selected as the collection muscle groups. The channel settings are shown in TABLE 2.

CH1-CH4 are sEMG acquisition sensors, with 2 patch electrodes placed along the muscle fibre direction at the muscle bulge, with a centre distance of about 20mm–30mm [29]. The reference electrode is placed at the electrically neutral articular bony prominence, which serves as the ground terminal for the signals. CH5 is a pressure sensor that is placed in the left hand and is used to record the onset and termination points of each movement to facilitate the classification of the subsequent movements, as shown in FIGURE 5(a).

Combined with the practical application of the developed upper limb rehabilitation robot, in order to realistically distinguish the subject’s upper limb movement intention, all of them selected the ADL movement of the shoulder joint forward movement to start the follow-up work, which is eating, touching the ear, and lifting up the hand, as shown in FIGURE 5 (b).

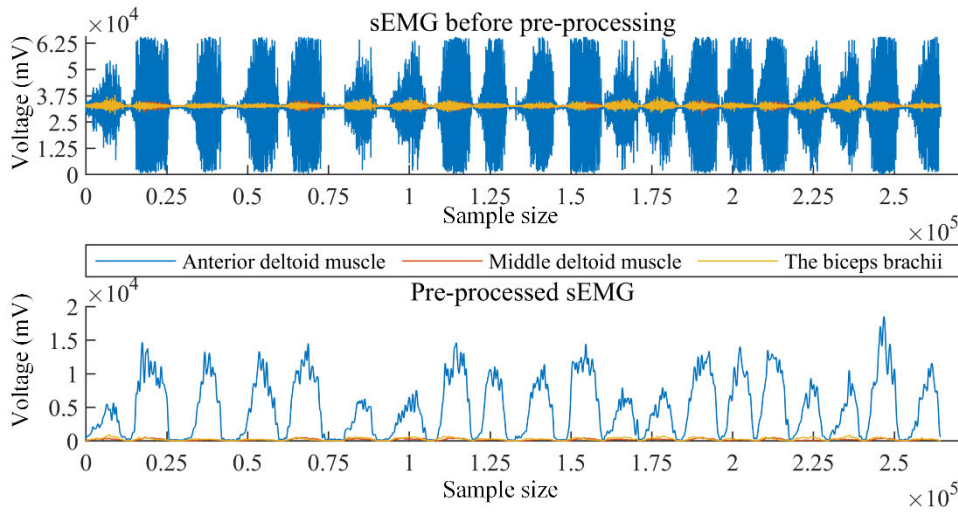


FIGURE 7. Comparison of signals before and after pre-processing.

TABLE 3. Feature description.

Features	Displayed Formula	Clarification	Exegesis
Time domain characteristics	$NAV = \frac{1}{N} \sum_{i=1}^N  x_i $	Detection of muscle contraction level and average intensity of sEMG signals	$x_i$ is the $i$ th sample of the signal; $N$ is the total number of samples of the signal; and $\mu$ is the mean of the signal.
	$RMS = \sqrt{\frac{1}{N} \sum_{i=1}^N x_i^2}$	sEMG RMS detection	
	$VAR = \frac{1}{N} \sum_{i=1}^N (x_i - \mu)^2$	Change in amplitude and severity of sEMG	
Frequency domain characteristic	$MPF = \frac{\sum_{i=1}^N f_i \cdot P(f_i)}{\sum_{i=1}^N P(f_i)}$	Mean value of corrected frequency of sEMG	$f_i$ is the $i$ th frequency component; $P(f_i)$ is the corresponding power spectral density; and $N$ is the total number of frequency components.
	$MF = f_m$ $\sum_{i=1}^m P(f_i) = \frac{1}{2} \sum_{i=1}^N P(f_i)$	Correcting the median frequency of the sEMG	

C. SEGMENTAL SEMG

In the signal acquisition process, six subjects were first trained in proficiency to memorise the termination position of each action segment, and the pressure sensor was used to record the start and termination positions of each action segment, thus obtaining the four sEMG sequences of each action. Figure 6(a) now shows the sEMG of the four segments of the drinking action, and Figure 6(b) shows the start and stop positions of each action.

We did not perform follow-up work on CH2 acquisition because the movements selected for this paper were all forward shoulder movements with very low triceps involvement and insignificant muscle activation. Each participant performed one set of experiments for each segment of each movement, for a total of four sets of experiments, with 20 ADL movements randomly acquired in each set. We ensured there was no muscle fatigue before performing the next set of acquisitions, with a 10-minute interval between each set.

D. PREPROCESSING

Most of the sEMG power was contained between 20 and 200 Hz, and the sEMG data from 20 to 450 Hz was filtered using a 4th-order Butterworth bandpass filter to reduce the effects of noise and motion artefacts. In addition, a 4th-order Butterworth filter with a cut-off frequency of 10 Hz was used for low-pass filtering and full-wave rectification to compute the envelope of the sEMG, and a comparison of the signals before and after complete motion preprocessing is shown in FIGURE 7.

E. FEATURE EXTRACTION AND DIMENSIONALITY REDUCTION

We need to extract features from preprocessed sEMG signals to increase the information density and improve the efficiency of upper limb movement classification. In this paper, the time domain features MAV, RMS, and variance (VAR) and the frequency domain features mean frequency (MF) and median power frequency (MPF) of segmented sEMG are extracted,

TABLE 4. Description of discrete indicators.

Discrete Indicator	Displayed Formula	Exegesis
Extremely Poor	$R = \max(S_i) - \min(S_i)$	$R$ denotes the extreme deviation, with a larger $R$ indicating a larger degree of dispersion, $S_i$ denotes the data magnitude.
Interquartile Distance	$Q = P_{x1} - P_{x2}$	$Q$ denotes the interquartile spacing, a set of data is arranged in ascending order, the number in the $x\%$ percentile is denoted by, and the greater the spacing of the $Q$ values indicates the greater the degree of dispersion.
Variance	$V = \frac{1}{N} \sum_{i=1}^N \left( S_i - \frac{1}{N} \sum_{i=1}^N S_i \right)^2$	$V$ denotes the variance, $N$ denotes the length of the data, and the larger $V$ the greater the degree of dispersion.

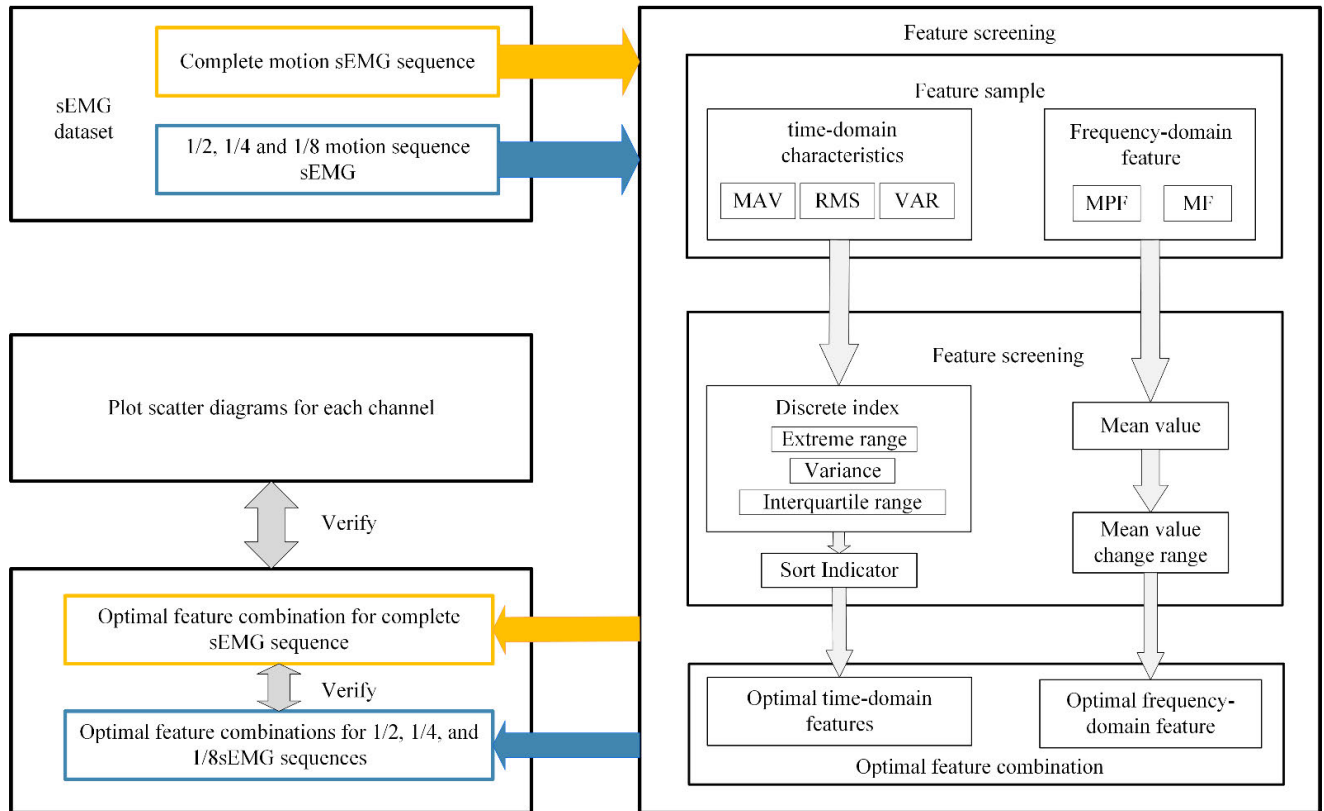


FIGURE 8. Feature extraction and dimension reduction process.

totalling five features, and the formula for each feature is as follows (TABLE 3):

The choice of eigenvalues is closely related to the outcome of action recognition, and too many eigenvalues will affect the computer’s decision-making speed. On the contrary, insufficient eigenvalues will cause the robot to fail to accurately acquire the patient’s limbs’ movement intention [30], [31]. In this paper, we propose to select one time domain feature and one frequency domain feature from the five extracted features for subsequent motion intent recognition.

For the screening of time domain features, the greater the dispersion of the feature value, the more favourable it is for the classification of motion intent recognition. Considering that a single discrete metric cannot fully represent the degree of signal discretization, three discrete metrics will be used to process the obtained feature values, namely, the extreme

TABLE 5. Ordering of discrete metrics for time-domain features.

CH	-	MAV	RMS	VAR	Order of Dispersion
CH1	R	-0.5285	-0.6249	1.1534	2、3、1
	Q	0.5873	0.5674	-1.1546	1、2、3
	V	0.6008	0.5536	-1.1544	1、2、3
CH2	R	-0.5766	-0.5781	1.1547	2、3、1
	Q	-0.568	-0.5867	1.1547	2、3、1
	V	-0.5768	-0.5779	1.1547	2、3、1
CH3	R	0.6325	0.5204	-1.1529	1、2、3
	Q	0.5866	0.568	-1.1547	1、2、3
	V	0.5958	0.5587	-1.1545	1、2、3

deviation, interquartile range, and variance, which can be expressed in TABLE 4. For the frequency domain features, the sEMG frequency domain features were extracted to take

TABLE 6. Test function description.

Function	Expression	Dim	Range	Optimal
Schwefel's Problem 2.22	$f_1(x) = \sum_{i=1}^n  x_i  + \prod_{i=1}^n  x_i $	30	[-10,10]	0
Step	$f_2(x) = \sum_{i=1}^n ([x_i + 0.5])^2$	30	[-100,100]	0
Ackley	$f_3(x) = -20 \exp\left(-0.2 \sqrt{\frac{1}{n} \sum_{i=1}^n x_i^2}\right) - \exp\left(\frac{1}{n} \sum_{i=1}^n \cos(2\pi x_i)\right) + 20 + e$	30	[-32,32]	0
Generalized Penalized	$f_4(x) = \frac{\pi}{n} \left\{ 10 \sin(\pi y_i) + \sum_{i=1}^{n-1} (y_i - 1)^2 [1 + 10 \sin^2(\pi y_{i+1}) + (y_n - 1)^2] \right\} + \sum_{i=1}^n u(x_i, 10, 100, 4)$ $y_i = 1 + \frac{x_i + 1}{4}, u(x, a, k, m) = \begin{cases} k(x_i - a)^m, & x_i > a \\ 0, & -a < x_i < a \\ k(-x_i - a)^m, & x_i < -a \end{cases}$	30	[50,50]	0
Kowalik	$f_5(x) = \sum_{i=1}^{11} \left[ a_i - \frac{x_4 (b_i^2 + b_i x_2)}{b_i^2 + b_i x_3 + x_4} \right]^2$	4	[-5,5]	0.1484
Shekel	$f_6(x) = -\sum_{i=1}^7 \left[ (X - a_i)(X - a_i)^T + c_i \right]^2$	4	[0,10]	-1

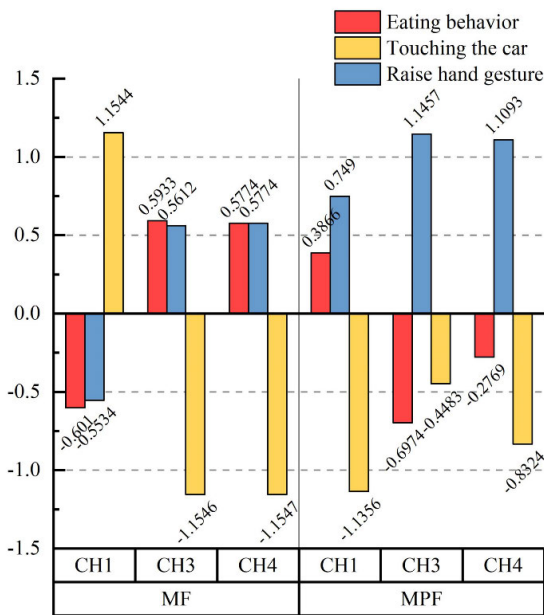


FIGURE 9. Frequency domain eigenaverage.

the mean value, the greater the change in the mean value, the more favourable it is for the classification of motion intent recognition.

The eigenvalue optimisation process is shown in FIGURE 8. The results of ranking the discrete degree of time domain features calculated for the subjects' full action sEMG are shown in TABLE 5. The results of comparing the mean values of the frequency domain features are shown in FIGURE 9. The optimal feature combination is selected after comprehensive consideration as MAV+MPF.

The scatter plots of the three channels are plotted separately, as shown in FIGURE 10. Since it is not easy for CH2 to

TABLE 7. Parameter setting of each algorithm.

Algorithm	Parameter Settings
GA	$pc = 0.9, pm = 0.2$
PSO	$c1 = c2 = 2, \omega_{Max} = 0.9, \omega_{Min} = 0.6$
SA	$TF = 10E-10$
SSA	$ST = 0.7; PD = 0.4; SD = 0.2$

distinguish between the three selected ADL actions, the subsequent work in this paper only analyses the MAV+MPF of the two channels, CH1 and CH4, for a total of 4-dimensional features.

#### IV. RESULTS AND DISCUSSION

##### A. COMPARISON OF OPTIMISATION ALGORITHMS

Compared with other optimisation algorithms, SSA has local optimum; and F5 and F6 are composite benchmark test functions to test the balancing ability of the algorithm in exploring and developing. Test benchmark functions are shown in TABLE 6.

Meanwhile, the genetic algorithm (GA), particle swarm optimisation algorithm (PSO), and simulated annealing algorithm (SA) are selected to compare the cross-sectional performance with the SSA [32], [33], [34]. The parameter settings of each algorithm are shown in TABLE 7, and the population size N of all algorithms is set to 50, the maximum number of iterations is set to 100, and the six test functions are run independently of each other. The process is repeated 30 times, and the statistical results are shown in TABLE 8. The optimal fitness value, the average fitness value, the worst fitness value, and the standard deviation are used as judgements of the standard algorithms' performance.

From the test results of unimodal test functions F1 and F2, SSA shows good convergence speed and optimisation



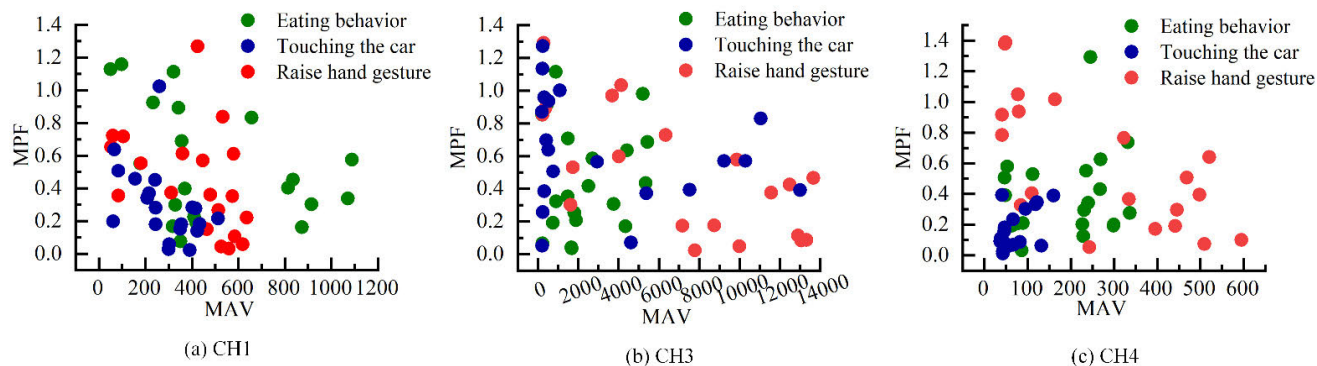


FIGURE 10. Feature combination scatter plot of each channel.

TABLE 8. Comparison of test benchmark function results.

Function	Algorithm	Optimal	Mean	Worst	Standard
F1	GA	0.35362	2.5174	10.9628	2.6083
	PSO	0.43734	0.93798	1.8565	0.39828
	SA	0.00063377	0.021801	0.19034	0.03714
	SSA	0	8.4389e-31	1.2382e-29	3.1224e-30
F2	GA	1.7001	18.6089	110.915	23.3712
	PSO	0.040611	0.25615	0.79999	0.16885
	SA	8.0119e-07	0.036419	0.52152	0.097749
	SSA	5.8563e-12	2.4701e-09	3.6796e-08	6.9367e-09
F3	GA	4.5762	13.0523	17.7345	3.2726
	PSO	0.58458	1.3192	2.3646	0.48006
	SA	0.0026345	3.5337	18.8316	4.8007
	SSA	8.8818e-16	8.8818e-16	8.8818e-16	0
F4	GA	0.0077995	1.9423	7.3496	1.9202
	PSO	0.0015955	0.012361	0.062299	0.014099
	SA	3.2965e-06	0.15968	1.3009	0.2789
	SSA	5.4231e-13	8.1815e-10	9.8996e-09	1.9298e-09
F5	GA	0.0011087	0.012036	0.031621	0.0099955
	PSO	0.00075144	0.0010742	0.0026943	0.00036155
	SA	0.0011089	0.013341	0.063313	0.013211
	SSA	0.00030749	0.00031003	0.00034673	7.559e-06
F6	GA	-1.9883	-1.0312	-0.57636	0.3675
	PSO	-10.4024	-7.1595	-2.7508	3.5565
	SA	-10.4029	-5.1004	-1.8376	3.3489
	SSA	-10.4029	-8.8084	-5.0877	2.4774

accuracy and can accurately optimise to the ideal value, and the optimisation results have obvious advantages over other optimisation algorithms. SSA finds the best value first for the multimodal test function F3. For the multimodal test function F4 and the composite benchmark test function F5, it can get rid of the local best and find the global best solution, which is a big advantage over the other three algorithms. And the standard deviation value is the smallest, indicating that SSA is more robust. For the composite benchmark test function F6, although the PSO algorithm can reach the theoretical optimum, SSA is faster in finding the optimum, and by comparing the mean and standard deviation, the stability of SSA's optimisation is significantly better than that of other algorithms. Comprehensive analysis shows that SSA has better performance and can be used as an optimisation algorithm for the motor intention recognition classifier. The average convergence curves of the six test functions are shown in FIGURE 11.

**B. COMPARISON OF MACHINE LEARNING MODELS**

Machine learning classification algorithms commonly used in motion intent recognition are generally SVM, Backpropagation Neural Network (BPNN), and ELM [35], [36], [37]. ELM is a newly developed supervised learning algorithm for single hidden layer feedforward neural networks with additive neurons. ELM learns much faster than traditional feedforward network learning algorithms than BPNN and has better generalisation performance [37]. ELM has become a popular tool for solving classification and regression problems.

This paper argues that the KELM algorithm optimised using the Gaussian kernel function is suitable for pattern recognition of motion intent. In order to verify the real-time effectiveness of KELM, four sets of motion datasets from each of the six subjects are taken, and the 4-dimensional combined features consisting of MAV+MPF are extracted and input into six commonly used classifiers such as SVM,

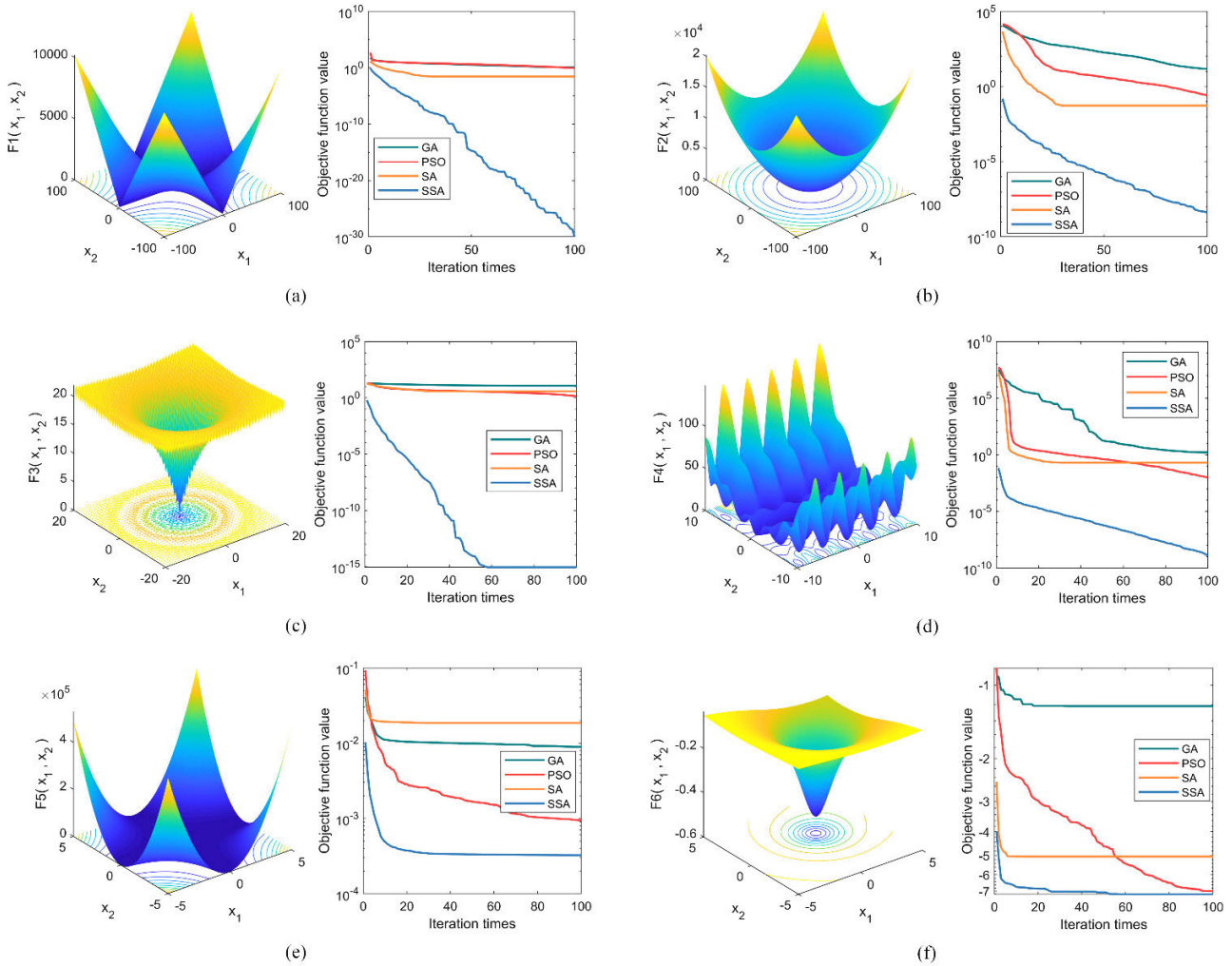


FIGURE 11. Test function average convergence curve.

Naïve Bayes (Bayes), BPNN, Long Short-Term Memory (LSTM), ELM, KELM and the training and testing process is repeated 30 times [38], [39]. All classifiers undergo 10 fold cross validation, with a training set ratio of 0.7. Different training and testing sets are repeatedly used as inputs, and the 10 validation results are averaged to ensure that the model achieves optimal performance.

From Fig. 12, it can be seen that SVM, ELM, and KELM all have good recognition accuracy, but the robustness of KELM is better than that of SVM and ELM. and KELM has the fastest rate of decrease in the running speed, and the running time is only slower than that of Bayes in the case of 1/8 action segment recognition, which indicates that the use of KELM is a fast and effective method for the classification of motion patterns based on segmented sEMG.

C. COMPARISON OF KELM AND SSA-KELM

The two parameters, regularisation coefficient  $c$  and kernel function parameters  $s$ , in KELM will directly affect its

TABLE 9. Comparison of recognition speed after optimisation.

Algorithm	1/8	1/4	1/2	Complete
KELM	0.0080	0.0180	0.0515	0.2030
SSA-KELM	0.0102	0.0177	0.0492	0.2125

recognition accuracy. Therefore, this paper employs the SSA algorithm to determine the optimality of these two parameters, subsequently constructing the SSA-KELM classification algorithm.

The motion dataset was input into SSA-KELM for training and testing, and the recognition accuracy of each motion is shown in FIGURE 12, and the running speed is shown in TABLE 9. It can be seen that, compared with the KELM algorithm, the SSA-KELM algorithm improves the recognition accuracy of each action segment, makes up for the defects of the KELM algorithm that the recognition accuracy of the 1/4 segment and 1/2 segment is not high, and maintains a fast running speed, which proves the feasibility of this algorithm,

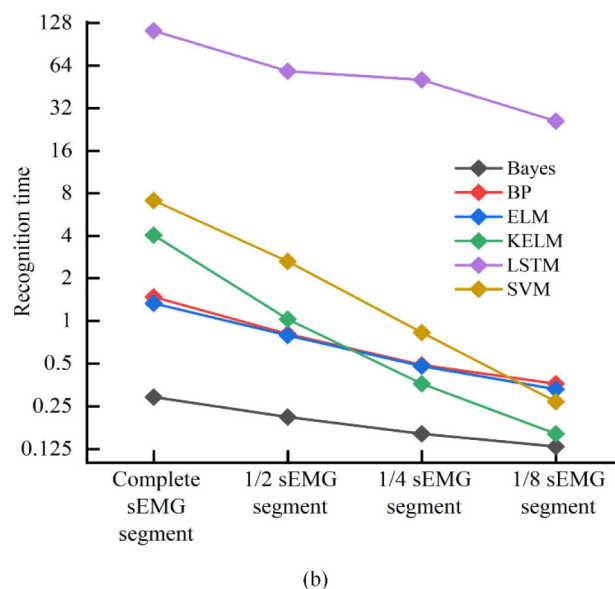
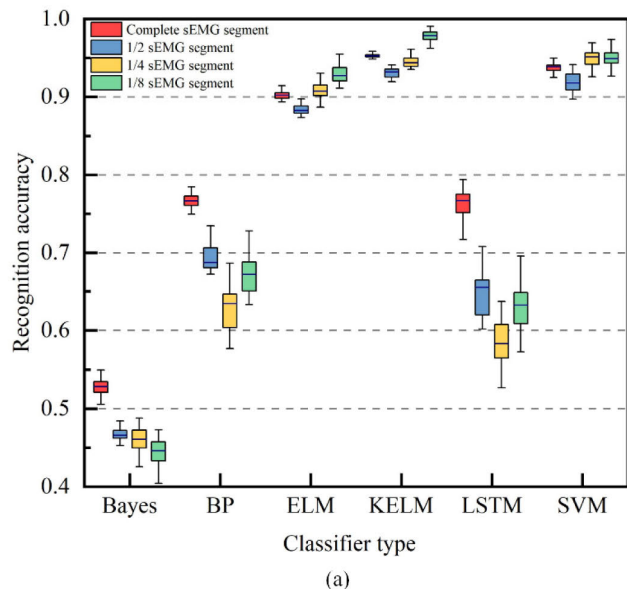


FIGURE 12. Classifier performance comparison.

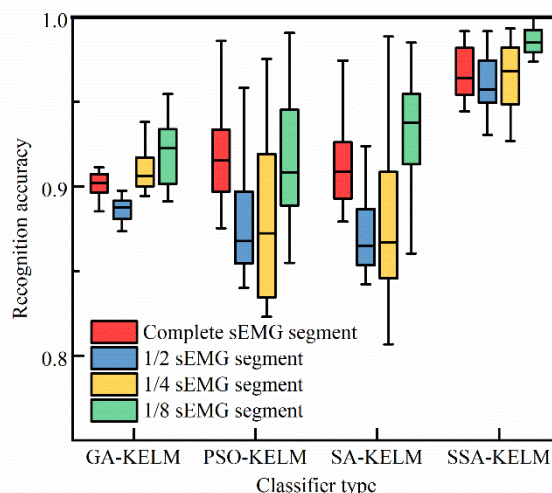
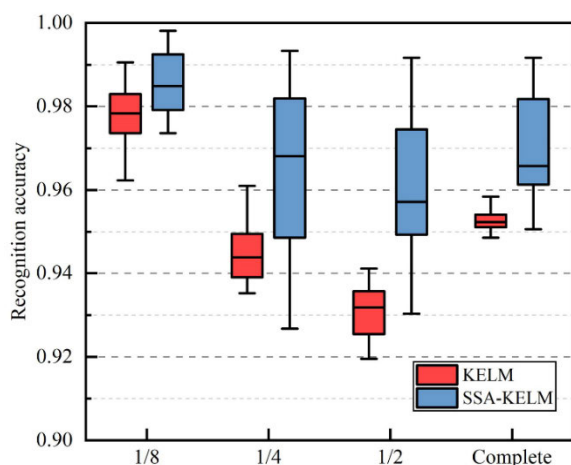


FIGURE 13. Comparison of recognition accuracy after optimization.

FIGURE 14. Optimisation of KELM parameters by different optimisation algorithms.

and it has a positive significance for the active-passive combination control of the rehabilitation robot.

**D. OPTIMISATION OF KELM BY DIFFERENT OPTIMISATION ALGORITHMS**

In order to verify the advantages of SSA-KELM, this paper uses different optimization algorithms to optimize the regularization coefficient  $c$  and the kernel function parameter  $s$  of KELM and compares the recognition accuracies of GA-KELM, PSO-KELM, SA-KELM, and SSA-KELM. SSA-KELM performed well and verified the feasibility of the method, as shown in FIGURE 14.

The parameter finding time of the optimization algorithm has been tested above using benchmark functions and will not be repeated here.

**V. CONCLUSION**

The development of active-passive combined control directly affects the patient’s postoperative recovery effect and is one of the key development directions for rehabilitation robots in the future. In this paper, we investigated the segmental surface EMG signals and identified the motor intention of 1/8, 1/4, and 1/2 sEMG segments of three ADL movements, which greatly restored the situation of stroke patients who could not realise the complete ADL movements at the early stage of rehabilitation due to muscle atrophy.

Accuracy and real-time prediction of active motor intention in patients with upper-limb motor dysfunction are the keys to robot-assisted rehabilitation. In this paper, we analyse

the time and frequency domain features of sEMG signals, screen the optimal feature combination MAV+MPF, and use the KELM classification model optimised by the SSA algorithm for training and prediction. The results demonstrate a significant improvement in the recognition accuracy of the SSA-KELM algorithm when compared to the traditional KELM algorithm. The algorithm achieves recognition accuracies as high as 98.3%, 96.8%, 95.7%, and 96.6% in 1/8, 1/4, 1/2, and complete sEMG sequences, demonstrating great superiority in the first segment. The recognition speed is guaranteed, and it is expected to be applied to the ADL action of the motor intention prediction study.

The selected ADL actions in this article are clearly distinguished in the early stages of the action, resulting in better recognition results for the classification model in smaller data segments. In future work, we will continue to verify the impact of different ADL actions on experimental results and apply this method to clinical experiments on upper limb rehabilitation robots to continuously optimize its applicability.

### CONFLICTS OF INTEREST

The authors have no relevant financial or non-financial interests to disclose.

### CREDIT AUTHORSHIP CONTRIBUTION STATEMENT

Mechanical design and prototype debug: Hao Yan and Xingao Li; conceptualisation and supervision: Hao Yan; data analysis and validation: Xingao Li, Zhongliang Shi, and Shuyuan Wang; the main content of this manuscript was created and written by Xingao Li and reviewed by all authors.

### DATA AVAILABILITY

The data will be made available upon reasonable request.

### ACKNOWLEDGMENT

(Hao Yan and Xingao Li contributed equally to this work.)

### REFERENCES

- [1] H. S. Markus, *Reducing Disability After Stroke*, vol. 17. Newbury Park, CA, USA: Sage, 2022, pp. 249–250.
- [2] M. J. Young, R. W. Regenhardt, T. M. Leslie-Mazwi, and M. A. Stein, “Disabling stroke in persons already with a disability: Ethical dimensions and directives,” *Neurology*, vol. 94, no. 7, pp. 306–310, Feb. 2020.
- [3] C. Yu, L. Luo, M. Li, J. Yu, R. Meng, and R. Yuan, “From the global views to understand the seriousness of the burden of stroke in China,” *J. Pub. Health Prev. Med.*, vol. 27, no. 1, pp. 1–5, 2016.
- [4] H. M. Qassim and W. Z. Wan Hasan, “A review on upper limb rehabilitation robots,” *Appl. Sci.*, vol. 10, no. 19, p. 6976, Oct. 2020.
- [5] X. Liang, W. Wang, Z. Hou, S. Ren, L. Peng, and J. Hu, “Interactive control methods for rehabilitation robot,” *Scientia Sinica Informationis*, vol. 48, no. 1, pp. 24–46, Jan. 2018.
- [6] L. Peng, Z. Hou, C. Wang, L. Luo, and W. Wang, “Physical interaction methods for rehabilitation and assistive robots,” *Acta Automatica Sinica*, vol. 44, no. 11, pp. 2000–2010, 2018.
- [7] X. Li, J. Liu, Y. Huang, D. Wang, and Y. Miao, “Human motion pattern recognition and feature extraction: An approach using multi-information fusion,” *Micromachines*, vol. 13, no. 8, p. 1205, Jul. 2022.
- [8] U. Coté-Allard, C. L. Fall, A. Campeau-Lecours, C. Gosselin, F. Laviolette, and B. Gosselin, “Transfer learning for sEMG hand gestures recognition using convolutional neural networks,” in *Proc. IEEE Int. Conf. Syst. Man, Cybern. (SMC)*, Oct. 2017, pp. 1663–1668.
- [9] Z. Li, B. Wang, C. Yang, Q. Xie, and C.-Y. Su, “Boosting-based EMG patterns classification scheme for robustness enhancement,” *IEEE J. Biomed. Health Informat.*, vol. 17, no. 3, pp. 545–552, May 2013.
- [10] W. Chen and Z. Zhang, “Hand gesture recognition using sEMG signals based on support vector machine,” in *Proc. IEEE 8th Joint Int. Inf. Technol. Artif. Intell. Conf. (ITAIC)*, May 2019, pp. 230–234.
- [11] R. A. R. C. Gopura, D. S. V. Bandara, K. Kiguchi, and G. K. I. Mann, “Developments in hardware systems of active upper-limb exoskeleton robots: A review,” *Robot. Auto. Syst.*, vol. 75, pp. 203–220, Jan. 2016.
- [12] Q. L. Li, Y. Song, and Z. G. Hou, “Estimation of lower limb periodic motions from sEMG using least squares support vector regression,” *Neural Process. Lett.*, vol. 41, no. 3, pp. 371–388, Jun. 2015.
- [13] R. Merletti, “The electrode–skin interface and optimal detection of bioelectric signals,” *Physiological Meas.*, vol. 31, no. 10, p. E01, Oct. 2010.
- [14] A. Pal, A. K. Gautam, and Y. N. Singh, “Evaluation of bioelectric signals for human recognition,” *Proc. Comput. Sci.*, vol. 48, pp. 746–752, Aug. 2015.
- [15] Y. N. Singh, S. K. Singh, and A. K. Ray, “Bioelectrical signals as emerging biometrics: Issues and challenges,” *ISRN Signal Process.*, vol. 2012, pp. 1–13, Jul. 2012.
- [16] P. Chen, H. Wang, H. Yan, J. Du, Y. Ning, and J. Wei, “sEMG-based upper limb motion recognition using improved sparrow search algorithm,” *Int. J. Speech Technol.*, vol. 53, no. 7, pp. 7677–7696, Apr. 2023, doi: 10.1007/S10489-022-03824-6.
- [17] J. Shi, Y. Cai, J. Zhu, J. Zhong, and F. Wang, “sEMG-based hand motion recognition using cumulative residual entropy and extreme learning machine,” *Med. Biol. Eng. Comput.*, vol. 51, no. 4, pp. 417–427, Apr. 2013.
- [18] Z. Lv, F. Xiao, Z. Wu, Z. Liu, and Y. Wang, “Hand gestures recognition from surface electromyogram signal based on self-organizing mapping and radial basis function network,” *Biomed. Signal Process. Control*, vol. 68, Jul. 2021, Art. no. 102629.
- [19] Y. Jiang, C. Chen, X. Zhang, C. Chen, Y. Zhou, G. Ni, S. Muh, and S. Lemos, “Shoulder muscle activation pattern recognition based on sEMG and machine learning algorithms,” *Comput. Methods Programs Biomed.*, vol. 197, Dec. 2020, Art. no. 105721.
- [20] Y. Yang, F. Duan, J. Ren, J. Xue, Y. Lv, C. Zhu, and H. Yokoi, “Performance comparison of gesture recognition system based on different classifiers,” *IEEE Trans. Cognit. Develop. Syst.*, vol. 13, no. 1, pp. 141–150, Mar. 2021.
- [21] X. Chen, Y. Li, R. Hu, X. Zhang, and X. Chen, “Hand gesture recognition based on surface electromyography using convolutional neural network with transfer learning method,” *IEEE J. Biomed. Health Informat.*, vol. 25, no. 4, pp. 1292–1304, Apr. 2021.
- [22] F. Wang, Z. Fan, K. Shi, and H. Wu, “Human upper limb movement recognition based on kernel principal component analysis and support vector machines,” in *Proc. 39th Chin. Control Conf. (CCC)*, Jul. 2020, pp. 3135–3140.
- [23] M. A. Vélez-Guerrero, M. Callejas-Cuervo, and S. Mazzoleni, “Artificial intelligence-based wearable robotic exoskeletons for upper limb rehabilitation: A review,” *Sensors*, vol. 21, no. 6, p. 2146, Mar. 2021.
- [24] L. Bi, A. Feleke, and C. Guan, “A review on EMG-based motor intention prediction of continuous human upper limb motion for human–robot collaboration,” *Biomed. Signal Process. Control*, vol. 51, pp. 113–127, May 2019.
- [25] C. Li, Y. Zhou, and Y. Li, “The signal processing and identification of upper limb motion based on sEMG,” *Wireless Pers. Commun.*, vol. 103, no. 1, pp. 887–896, Nov. 2018.
- [26] A. Chakraborty and A. K. Kar, “Swarm intelligence: A review of algorithms,” in *Nature-Inspired Computing and Optimization: Theory and Applications*, S. Patnaik, X.-S. Yang, and K. Nakamatsu Eds. Cham, Switzerland: Springer, 2017, pp. 475–494.
- [27] J. Xue and B. Shen, “A novel swarm intelligence optimization approach: Sparrow search algorithm,” *Syst. Sci. Control Eng.*, vol. 8, no. 1, pp. 22–34, Jan. 2020.
- [28] X. Ma, C. Wang, R. Zhang, and X. Wu, “A real-time gait switching method for lower-limb exoskeleton robot based on sEMG signals,” in *Proc. Int. Conf. Cogn. Syst. Signal Process.*, Nov. 2018, pp. 511–523.
- [29] D.-M. Wu, X. Sun, and Z.-C. Zhang, “Feature collection and analysis of surface electromyography signals,” *Chin. J. Tissue Eng. Res.*, vol. 14, no. 43, p. 8073, 2010.
- [30] W. Jia, M. Sun, J. Lian, and S. Hou, “Feature dimensionality reduction: A review,” *Complex Intell. Syst.*, vol. 8, no. 3, pp. 2663–2693, 2022.

[31] R. Zebari, A. Abdulazeez, D. Zeebaree, D. Zebari, and J. Saeed, "A comprehensive review of dimensionality reduction techniques for feature selection and feature extraction," *J. Appl. Sci. Technol. Trends*, vol. 1, no. 1, pp. 56–70, May 2020.

[32] J. H. Holland, "Genetic algorithms," *Sci. Amer.*, vol. 267, no. 1, pp. 66–73, 1992.

[33] J. Kennedy and R. Eberhart, "Particle swarm optimization," in *Proc. ICNN'95-Int. Conf. Neural Netw.*, 1995, pp. 1942–1948.

[34] P. J. Van Laarhoven, E. H. Aarts, and P. J. van Laarhoven, *Simulated Annealing*. Cham, Switzerland: Springer, 1987.

[35] M. A. Hearst, S. T. Dumais, E. Osuna, J. Platt, and B. Scholkopf, "Support vector machines," *IEEE Intell. Syst. Appl.*, vol. 13, no. 4, pp. 18–28, 1998.

[36] R. Hecht-Nielsen, "Theory of the backpropagation neural network," in *Neural Networks for Perception*. Amsterdam, The Netherlands: Elsevier, 1992, pp. 65–93.

[37] G.-B. Huang, Q.-Y. Zhu, and C.-K. Siew, "Extreme learning machine: Theory and applications," *Neurocomputing*, vol. 70, nos. 1–3, pp. 489–501, Dec. 2006.

[38] S. Hochreiter and J. Schmidhuber, "Long short-term memory," *Neural Comput.*, vol. 9, no. 8, pp. 1735–1780, Nov. 1997.

[39] I. Rish, "An empirical study of the naive Bayes classifier," in *Proc. IJCAI Workshop Empirical Methods Artif. Intell.*, 2001, no. 22, pp. 41–46.



**XINGAO LI** received the B.S. degree in mechanical engineering from Hebei University of Engineering, Handan, China, where he is currently pursuing the M.S. degree in mechanical engineering.

His research interests include mechanisms, robotics, and human motion signal classification.



**ZHONGLIANG SHI** received the B.S. degree in mechanical engineering from Hebei University of Water Resources and Electric Engineering, Cangzhou, China. He is currently pursuing the M.S. degree in mechanical engineering with Hebei University of Engineering, Handan, China.

His research interest includes the compliance control of upper limb rehabilitation manipulators.



**HAO YAN** received the B.S., M.S., and Ph.D. degrees in mechanical engineering from Yanshan University, Qinhuangdao, China.

He is currently a Lecturer with the College of Mechanical and Equipment Engineering, Hebei University of Engineering, Handan, China. His research interests include medical service robots, machine learning, and intelligent control algorithms for robots.



**SHUYUAN WANG** is currently pursuing the B.S. degree in robot engineering with Hebei University of Engineering, Handan, China.

His research interests include medical service robots and neural network algorithms.

...